ACS APPLIED MATERIALS & INTERFACES

Research Article

www.acsami.org

A Pronounced Dispersion Effect of Crystalline Silicon Nanoparticles on the Performance and Stability of Polymer:Fullerene Solar Cells

Joonhyeon Kim,[†] Seungsoo Lee,[†,‡] Sungho Nam,[†] Hyena Lee,[†] Hwajeong Kim,*[,†,§] and Youngkyoo Kim*[,†]

[†]Organic Nanoelectronics Laboratory, Department of Chemical Engineering, and [§]Research Institute of Advanced Energy Technology, Kyungpook National University, Daegu 702-701, Republic of Korea

[‡]Electronic Materials R&D Center, Dongwoo Fine-Chem Co. Ltd., Iksan-si, Chunbuk 570-140, Republic of Korea

Supporting Information

ABSTRACT: We investigated the dispersion effect of crystalline silicon nanoparticles (SiNP) on the performance and stability of organic solar cells with the bulk heterojunction (BHJ) films of poly(3-hexylthiophene) (P3HT) and [6,6]-phenyl-C_{61}-butyric acid methyl ester ($PC_{61}BM$). To improve the dispersion of SiNP in the BHJ films, we attached octanoic acid (OA) to the SiNP surface via esterification reaction and characterized it with Raman spectroscopy and high-resolution transmission electron microscopy. The OA-attached SiNP (SiNP-OA) showed improved dispersion in chlorobenzene without change of optical absorption, ionization potential and crystal nanostructure of SiNP. The device performance was significantly deteriorated upon high loading of SiNP (10 wt %), whereas relatively good performance was maintained without large degradation in the case of SiNP-OA. Compared to the control device (P3HT:$PC_{61}BM$), the device performance was improved by adding 2 wt % SiNP-OA, but it was degraded by adding 2 wt % SiNP. In particular, the device stability (lifetime under short time exposure to 1 sun condition) was improved by adding 2 wt % SiNP-OA even though it became significantly decreased by adding 2 wt % SiNP. This result suggests that the dispersion of nanoparticles greatly affects the device performance and stability (lifetime).

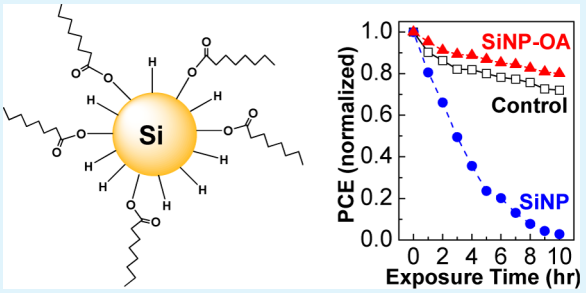

KEYWORDS: *organic solar cell, silicon nanoparticle, esterification, P3HT, stability*

INTRODUCTION

A keen interest has been recently paid to organic solar cells since early pioneering works for realizing the primitive photovoltaic functions of organic semiconducting materials.[1−4] In addition to the introduction of bulk heterojunction (BHJ) concept,[2−4] the encouraging breakthrough (ca. 2−2.5% power conversion efficiency (PCE)) can be ascribed to the finding of nanomorphology effects on the charge transport in the polymeric BHJ films.[5] Further improvement (3−5% PCE) could be enabled by employing regioregular poly(3-hexylthiophene) (P3HT) that undergoes a particular self-organizing behavior upon thermal and/or solvent annealing.[6−16] Although low-band gap polymers delivered 6−8% PCE very recently (single stack devices),[17−19] the PCE value of the P3HT-based solar cells has reached ∼6.5% by replacing the electron-accepting component (typically, [6,6]-phenyl-C_{61}-butyric acid methyl ester ($PC_{61}BM$)) with other fullerene derivatives that have shifted (toward vacuum level) lowest unoccupied molecular orbital (LUMO) energy levels leading to the increased open circuit voltages (V_{OC}).[20,21] Thus the P3HT polymer is still extensively used as an electron donor in polymer solar cell researches.

In the meantime to concentrate on improving the PCE values in polymer solar cells, the stability (lifetime) issue has been raised to the surface in a viewpoint of solar cell commercialization.[22−24] Four major factors have been so far pointed out to affect the stability of BHJ polymer solar cells: (1) Moisture and oxygen attacks to the organic layers and/or metal electrodes, (2) strong acidity effects of hole-collecting buffer layer (poly(3,4-ethylenedioxythiophene):poly(styrenesulfonate) (PEDOT:PSS)), (3) chemical degradation of organic materials in the BHJ layer, and (4) morphological instability in the BHJ layer. The first environmental issue has been resolved by applying a hermetic encapsulation as used for organic light-emitting devices,[25,26] whereas the strong acidity problem of PEDOT:PSS could be overcome by treating with a strong base and/or by replacing with other buffer layers.[27−30] The chemical degradation of electron-donating polymers can be also prevented by removing oxygen molecules that convert to a reactive singlet oxygen moiety to attack the pi-electrons in conjugated polymers under illumination (UV light in

Received: July 6, 2012
Accepted: September 13, 2012
Published: October 1, 2012

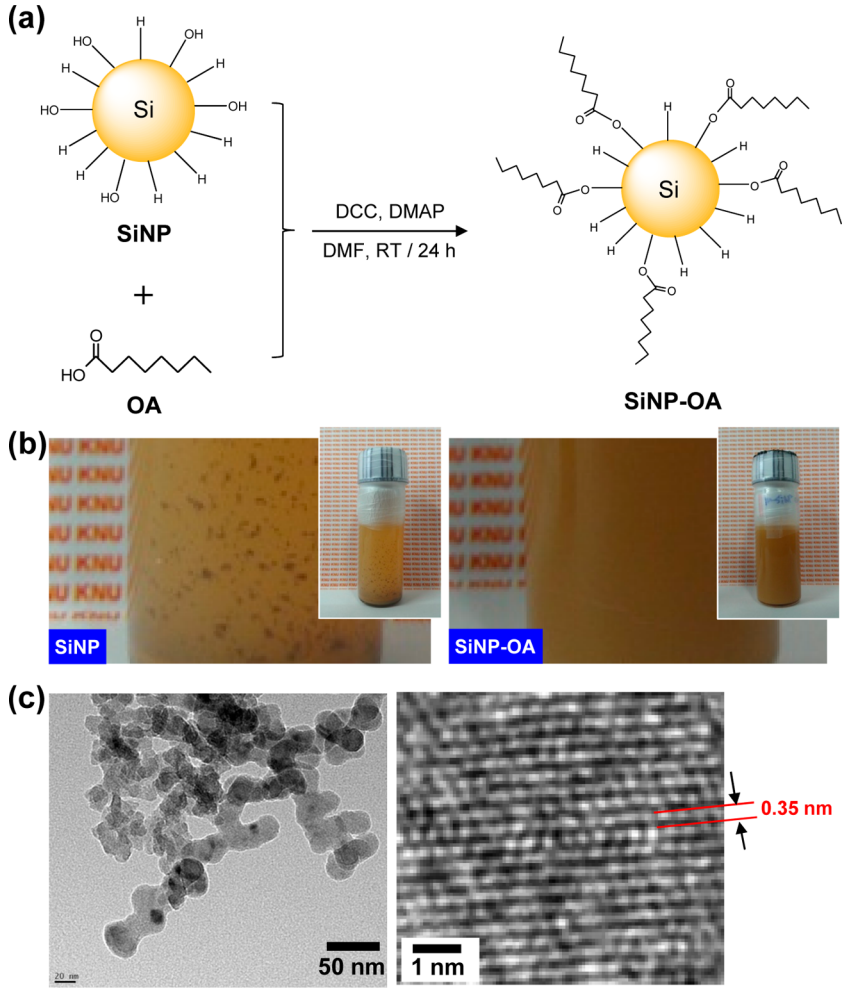

Figure 1. (a) Scheme for the esterification reaction between SiNP and octanoic acid (OA) leading to SiNP-OA. (b) Photographs for the solutions with SiNP (left) and SiNP-OA (right) in chlorobenzene: The SiNP solution shows big aggregates, whereas almost no aggregation is observed for the SiNP-OA solution. (c) HRTEM images for the SiNP-OA samples on the Cu grid (400 mesh).

general).[31,32] However, the last morphological instability issue is still debating because the BHJ morphology is delicately different depending on the material combination (mixing condition) between electron donors and electron acceptors. Recently, we reported that the stabilization of BHJ morphology is of importance to achieve the longer lifetime in the P3HT:$PC_{61}BM$ solar cells.[33,34]

In this work, as an alternative idea for the stability improvement in the BHJ polymer solar cells, we tried to add inorganic nanoparticles to the P3HT:$PC_{61}BM$ films because inorganic materials are typically more stable than organic materials.[35,36] To not degrade the semiconducting (electrical) property of the BHJ films as well as the charge separation balance between electron donor (P3HT) and electron acceptor ($PC_{61}BM$), we employed crystalline silicon nanoparticles (SiNP) because they are a well-known inorganic semiconductor with a similar valence band energy to the highest unoccupied molecular orbital (HOMO) energy of P3HT so that the hole charge carrier transport at least cannot be severely degraded.[37,38] In particular, we attached alkyl groups to the surface of SiNP via an esterification reaction in order to bestow better solubility (dispersion) in chlorobenzene solvent, which can lead to better dispersion quality of the inorganic nanoparticles in the BHJ films.

RESULTS AND DISCUSSION

As shown in Figure 1a, the chemical modification of SiNP was performed to attach the octanoic acid (OA) unit to the surface of SiNP. The esterification reaction between the hydroxyl group (OH) in SiNP and the carboxylic acid group (COOH) in OA was activated by the aid of mediators (DCC and DMAP).[39,40] After the esterification reaction, the modified SiNP (SiNP-OA) became noticeably well-dispersed in chlorobenzene solvent (see Figure 1b right), even though the original SiNP was aggregated and precipitated on the bottom of vial (see Figure 1b left). The shape and size of SiNP was found to be almost well maintained even after the esterification reaction (Figure 1c left). In addition, the crystalline nanostructure (Si−Si crystal lattices) of SiNP-OA was also clearly measured by a high resolution transmission electron microscope (HRTEM) (Figure 1c right).[41] This result supports that the present chemical modification process successfully endowed SiNP with good solubility (dispersion) in chlorobenzene solvent without alteration of the original SiNP nanostructure.

To further confirm the attachment of OA unit to the SiNP surface via the esterification reaction, we employed the Raman spectroscopy technique ,which can detect the presence of the atoms in the unique functional groups (C═O and C−H) in

dx.doi.org/10.1021/am301250s | ACS Appl. Mater. Interfaces 2012, 4, 5300−5308

the OA unit. First, we checked the status of Si−Si bonds in the SiNP before and after the esterification reaction. As shown in Figure 2a, the Si−Si bonds (crystalline Si) were measured at the

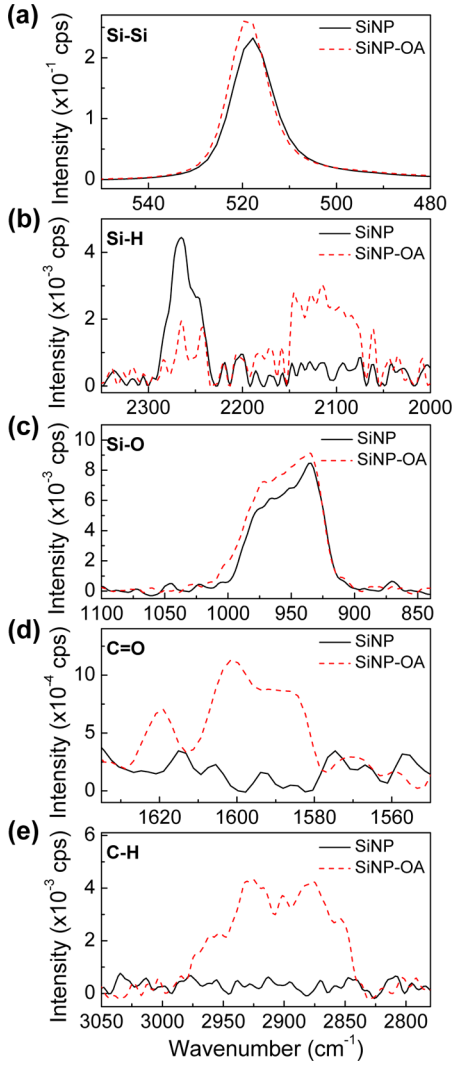

Figure 2. Raman spectra of SiNP and SiNP-OA powders spread on quartz substrates: (a) Si−Si, (b) Si−H, (c) Si−O, (d) C═O, and (e) C−H. The excitation wavelength was 1064 nm (Nd:YAG laser).

almost same wavenumber, indicating no particular change in the Si−Si linkage and crystal structures as discussed in Figure 1c (we note that the Raman intensity difference between SiNP and SiNP-OA is attributed to the different amount of samples loaded for the Raman spectrum measurement). However, the Si−H bonds were influenced by the esterification reaction because the original peaks (2240−2280 cm^{-1}) in the SiNP were decreased while new peaks at around 2100 cm^{-1} were emerged (Figure 2b). This Si−H bond change implies that the surface environment of SiNP was changed upon the esterification reaction. Because the Si−OH groups are naturally made on the surface (Si−H groups) of SiNP in the air ambient condition,[42] the S−H peak change can be explained by the formation of Si−OH groups during the esterification reaction even though the quantitative analysis is impossible for the present Raman spectroscopy system (see the Si−O Raman peaks in Figure 2c). Anyhow, the clear evidence for the OA unit attachment on the surface of SiNP is provided from the presence of the C═O peak in SiNP-OA, whereas no C═O peak was measured for the original SiNP sample (see Figure 2d). In addition, the C−H peak was also measured for the SiNP-OA sample even though the original SiNP sample showed no C−H peak (Figure 2e).

Then the optical absorption spectra of SiNP and SiNP-OA were measured by using poly(methyl methacrylate) (PMMA) as a host film where SiNP or SiNP-OA were dispersed, because the unstable solution phases (time-dependent gradual change in solution concentration by aggregation and sedimentation) could not deliver a reproducible result in the case of SiNP. As shown in Figure 3a, the spectral shape was almost not

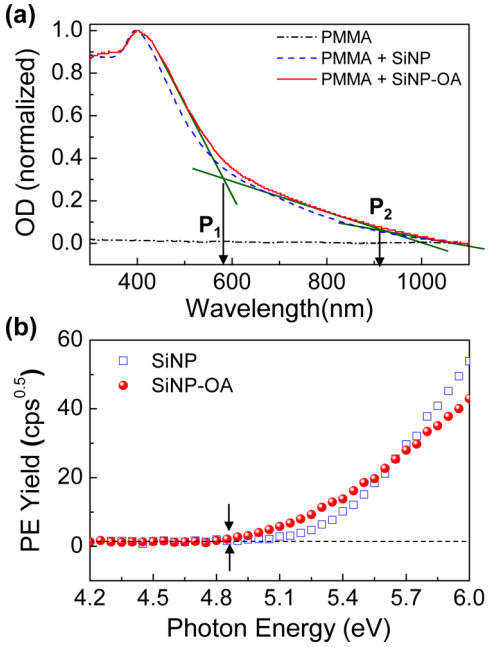

Figure 3. (a) UV−visible absorption spectra of films coated on quartz substrates: The optical density (OD) was normalized for exact comparison, whereas P_1 and P_2 denote the onset points of each zone. (b) Photoelectron (PE) yield spectra of SiNP and SiNP-OA powders spread on quartz substrates; the black arrows denote the onset point of PE yield.

changed after the esterification reaction. From the two major slopes at a boundary of ca. 600 nm in the absorption spectra (note that the edge tails above 900 nm can be assigned to the optical attenuation/scattering effect of medium), we can get two onset points (P_1 = 585 nm and P_2 = 910 nm) which correspond to the optical band gap energies (P_1 = 2.1 eV and P_2 = 1.4 eV). Similarly, the onset points (ca. 4.86 eV) in the photoelectron yield (PEY) spectra were almost not changed between SiNP and SiNP-OA even though the PEY trend according to the photon energy was slightly changed after the esterification reaction (Figure 3b). After calibration based on the reference material (see Figure S1 in the Supporting Information),[43,44] we obtained the valence band energy of SiNP-OA as ∼5.2 eV. From the optical band gaps the conduction band energy values can be calculated to 3.1 eV (from P_1 in Figure 3a) and 3.8 eV (from P_2 in Figure 3a), but the higher value (3.8 eV) is assigned as the actual conduction band energy (crystalline Si−Si) that corresponds to the lowest unoccupied molecular orbital (LUMO) energy in organic semiconductors.

Next, we fabricated solar cells with the P3HT:PC$_{61}$BM films that contain SiNP or SiNP-OA of which content was varied

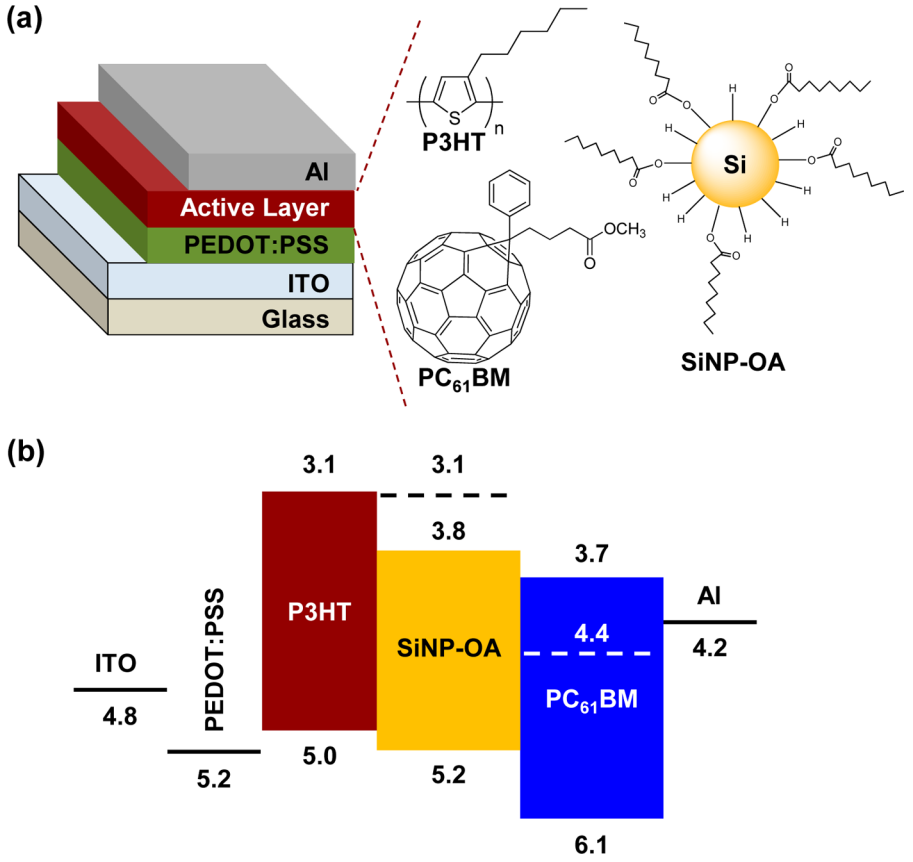

Figure 4. (a) Device structure of the P3HT:$PC_{61}BM$ solar cells with SiNP or SiNP-OA (Note that the SiNP structure was omitted). (b) Energy band diagram of the P3HT:$PC_{61}BM$ solar cells with SiNP-OA: The negative sign and "eV" unit were omitted to avoid crowding the illustration.

from 0 wt % to 10 wt % on the basis of the total weight (51 mg) of P3HT:$PC_{61}BM$ (1:0.7 by weight) (see Figure 4a). Here, considering the energy band diagram (Figure 4b), which was built on the basis of the valence and conduction band energies obtained in Figure 3, it is understood that the charge separation process can also occur at the interface between P3HT and SiNP-OA(or SiNP) though the offset (0.7 eV) between P3HT and SiNP-OA is smaller than that (0.9 eV) between P3HT and $PC_{61}BM$. Therefore, the presence of SiNP-OA or SiNP is expected to influence on the performance of solar cells via cascade charge (electron) transport from P3HT to SiNP-OA (or SiNP) and then to $PC_{61}BM$. This will be discussed again in the optimized devices.

As shown in Figure 5a, the shape of the current density–voltage (J–V) curves was slightly changed as the SiNP content increased up to 4 wt %. However, further addition of SiNP (10 wt %) did hugely deteriorate the J–V curve shape, leading to extremely low fill factor (FF = 16.7% from 45.1% for control device) (see Table 1). In addition, the short circuit current density (J_{SC}) was greatly reduced by ca. 41% from 9.3 mA/cm^2 (control device) to 5.5 mA/cm^2 (10 wt % SiNP), while the open circuit voltage (V_{OC}) was relatively slightly decreased (from 0.62 to 0.59 V). In contrast, the J–V curve shape was not significantly changed when 10 wt % SiNP-OA was added to the P3HT:$PC_{61}BM$ film, whereas the V_{OC} position was not changed at all even though the J_{SC} value was slightly decreased by ca. 13% from 9.3 mA/cm^2 (control device) to 8.1 mA/cm^2 (10 wt % SiNP-OA) (see Figure 5b and Table 1). In particular, a close look at the J-V curve can find that the J-V curve shape became even better for the device with 2 wt % SiNP-OA (note

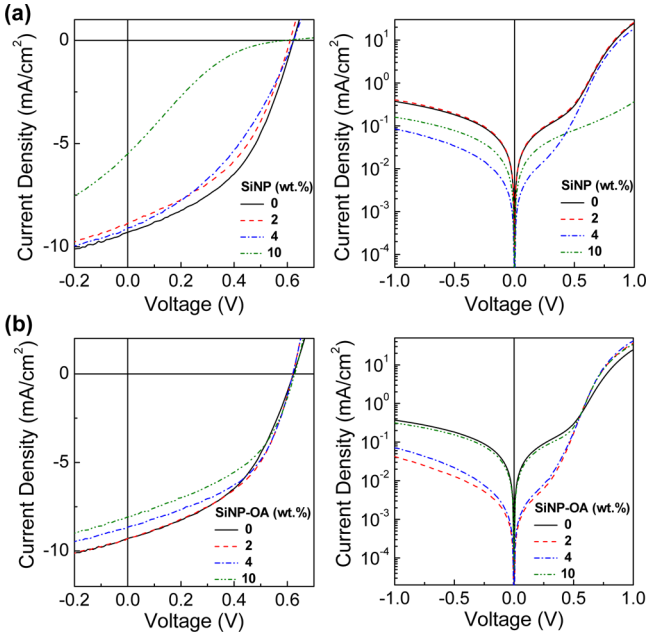

Figure 5. (a) J–V curves of the P3HT:$PC_{61}BM$ solar cells with various SiNP contents under 1 sun (left) and in the dark (right). (b) J–V curves of the P3HT:$PC_{61}BM$ solar cells with various SiNP-OA contents under 1 sun (left) and in the dark (right).

that the FF value was improved from 45.1% (control device) to 46.6% (2 wt % SiNP-OA). The different trend between SiNP and SiNP-OA can be primarily attributed to the different charge

dx.doi.org/10.1021/am301250s | ACS Appl. Mater. Interfaces 2012, 4, 5300–5308

Table 1. Performance Summary of the P3HT:$PC_{61}BM$ Solar Cells with SiNP (A) or SiNP-OA (B): The 'C_{NP}" Denotes the Concentration of the Silicon Nanoparticles

	J_{SC} (mA/cm^2)		V_{OC} (V)		FF (%)		PCE (%)		R_S (kΩ cm^2)	
C_{NP} (wt %)	A	B	A	B	A	B	A	B	A	B
0	9.3		0.62		45.1		2.6		0.25	
2	8.9	9.3	0.61	0.62	43.3	46.6	2.3	2.7	0.25	0.18
4	9.1	8.7	0.62	0.62	38.2	48.0	2.2	2.6	0.33	0.18
10	5.5	8.1	0.59	0.62	16.7	45.3	0.5	2.3	7.94	0.22

transport because the dark $J-V$ curve was severely deformed for the device with 10 wt % SiNP, whereas the dark $J-V$ curve was even better for the device with 10 wt % SiNP-OA than the control device (see higher forward current density at above open circuit condition). The charge transport change is also proven by the drastic jump of series resistance (R_S) for the devices with SiNP (see Table 1). Here we can speculate that the different charge transport might be closely related with the film morphology when it comes to the poor solubility of SiNP in chlorobenzene (see Figure 1b).[5,10]

Hence we tried to examine the nanoparticle-aggregation (degree of dispersion) morphology of the P3HT:$PC_{61}BM$ film with SiNP or SiNP-OA by employing a high-magnification optical microscope that enables observation on a scale of several tens of nanometers. As shown in Figure 6a, the control film (P3HT:$PC_{61}BM$) did not show any noticeable morphology, indicating that no big aggregates have been made between P3HT and $PC_{61}BM$.[33,34,45,46] When a small amount of SiNP or SiNP-OA (2 wt %) was added, tiny aggregates were observed for both cases but the film with SiNP-OA showed relatively better dispersion morphology (Figure 6b and 6c). As the SiNP (SiNP-OA) content increased further, the film with SiNP-OA showed much finer morphology (less aggregation) than that with SiNP (Figure 6d–g). This result evidence that the attachment of OA groups to the SiNP surface indeed help better dispersion of SiNP nanoparticles in the P3HT:$PC_{61}BM$ film.

Next, the influence of nanoparticle addition on the nanostructure of P3HT domains was investigated with a grazing incidence X-ray diffraction (GIXD) technique.[16,33,46] As shown in Figure 7a (see Figure 3c for the representative 2D image for the control film and Figure S2 in the Supporting Information for all 2D images), the characteristic (100) diffraction peaks of P3HT were measured for all films regardless of the nanoparticle contents in the direction of both out-of-plane (OOP) and in-plane (IP). In addition, the high order diffraction peaks ((200) and (300)), representing the longer range ordering of P3HT chains, were also found for all films. From this apparent analysis, it seems that the addition of Si nanoparticles do not significantly affect the crystallization of P3HT chains. However, we find that the intensity ratio of (200) to (100) peaks in the OOP direction was much lower for SiNP-OA than SiNP (see Figure 7b). This result informs that the long-range ordering of P3HT chains was more considerably disturbed by the presence of SiNP-OA than SiNP, indicating better dispersion of SiNP-OA than SiNP in the P3HT:$PC_{61}BM$ films. This conclusion can be partly supported by the result that the optical absorption intensity at around 600 nm (wavelength), which is related with the intermolecular stacking of P3HT chains, was relatively more increased by the addition of SiNP than SiNP-OA (see Figure S6 in the Supporting Information). Therefore, we suggest that the dispersion state

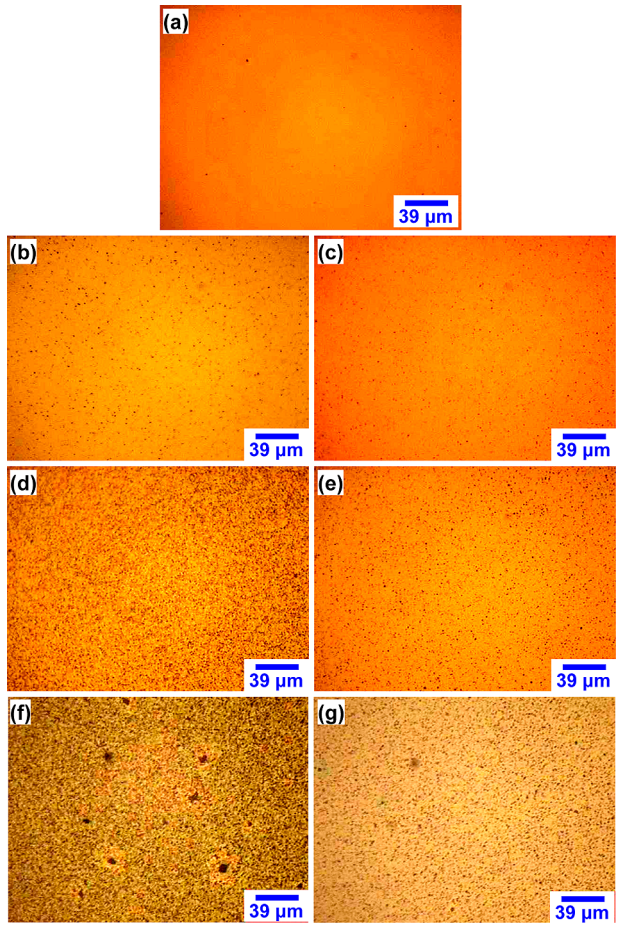

Figure 6. Optical microscope images for the BHJ films coated on the PEDOT:PSS/ITO-glass substrates: (a) P3HT:$PC_{61}BM$ (1:0.7 by weight), (b) P3HT:$PC_{61}BM$ with 2 wt % SiNP, (c) P3HT:$PC_{61}BM$ with 2 wt % SiNP-OA, (d) P3HT:$PC_{61}BM$ with 4 wt % SiNP, (e) P3HT:$PC_{61}BM$ with 4 wt % SiNP-OA, (f) P3HT:$PC_{61}BM$ with 10 wt % SiNP, and (g) P3HT:$PC_{61}BM$ with 10 wt % SiNP-OA.

of Si nanoparticles indeed affects the nanostructure of P3HT chain ordering in the BHJ films.

On the basis of the above results, we carried out the device optimization to achieve better performance in the P3HT:$PC_{61}BM$ solar cells with SiNP or SiNP-OA. Because adding 2 wt % SiNP-OA resulted in the improved device performance as discussed in Figure 5 (see also Table 1), we concentrated on this composition for the device optimization. As shown in Figure 8a, the optimized device with 2 wt % SiNP (PCE = 3.5%) was still slightly inferior to the control device (PCE = 3.6%) though several tens of optimization experiments have been performed. This inferior performance is basically attributed to the low FF owing to the relatively coarser morphology leading to the slightly poor charge transport in the

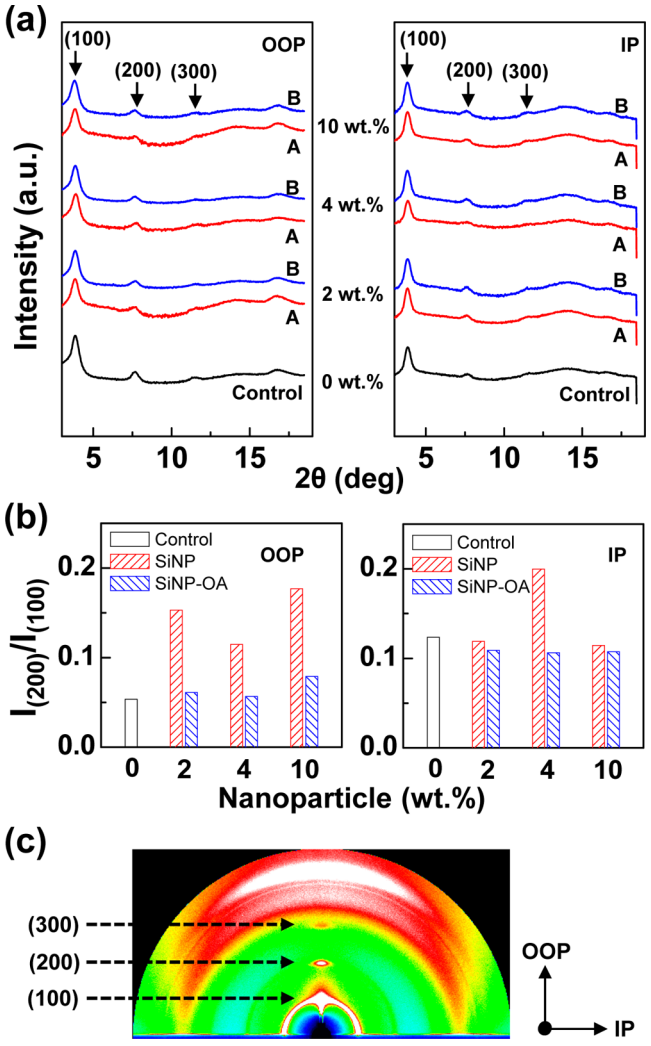

Figure 7. (a) 1D GIXD profiles for the BHJ films coated on the PEDOT:PSS/ITO-glass substrates: (control) P3HT:$PC_{61}BM$ (1:0.7 by weight), (A) P3HT:$PC_{61}BM$ with SiNP, (B) P3HT:$PC_{61}BM$ with SiNP-OA. (b) Intensity ratio ($I_{(200)}/I_{(100)}$) of (200) peaks to (100) peaks in the 1D GIXD profiles. (c) Representative 2D GIXD image and notations for each diffraction spot.

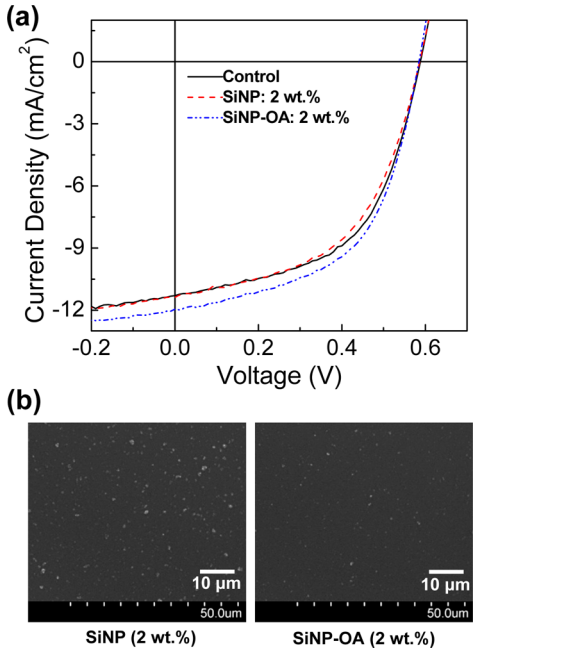

Figure 8. (a) Light $J-V$ curves of the optimized P3HT:$PC_{61}BM$ solar cells with 2 wt % SiNP or 2 wt % SiNP-OA. (Control device P3HT:$PC_{61}BM$): J_{SC} = 11.3 mA/cm^2, V_{OC} = 0.58 V, FF = 55%, PCE = 3.6%, R_S = 0.12 kΩ cm^2, R_{SH} = 2.6 kΩ cm^2; (P3HT:$PC_{61}BM$:SiNP_2 wt %): J_{SC} = 11.3 mA/cm^2, V_{OC} = 0.58 V, FF = 52%, PCE = 3.5%, R_S = 0.13 kΩ cm^2, R_{SH} = 2.2 kΩ cm^2; (P3HT:$PC_{61}BM$:SiNP-OA_2 wt %): J_{SC} = 12 mA/cm^2, V_{OC} = 0.58 V, FF = 55%, PCE = 3.8%, R_S = 0.1 kΩ cm^2, R_{SH} = 3.9 kΩ cm^2. (b) SEM images of the P3HT:$PC_{61}BM$ films with 2 wt % SiNP or 2 wt % SiNP-OA used for the optimized solar cells: The enlarged images are shown in Figure S3 in the Supporting Information.

active layer (see the scanning electron microscope (SEM) images in Figure 8b), because the J_{SC} and V_{OC} values were unchanged (see Figure 8 caption). However, the optimized device with 2 wt % SiNP-OA exhibited higher PCE (3.8%), which can be attributed to the enhanced J_{SC} value without expense of other parameters compared to the control device (note that the shunt resistance (R_{SH}) was also improved for the device with SiNP-OA). In particular, the dispersion morphology of SiNP-OA was noticeably finer than that of SiNP (see Figure 8b right and Figure S3 in the Supporting Information). Here the slightly increased J_{SC} value can be ascribed partly to the additional charges generated at the interface between P3HT and SiNP-OA because the offset energy between the conduction band energy of SiNP-OA and the LUMO energy of P3HT is sufficiently large for taking electrons from the excitons made in the P3HT domains (see the energy band diagram in Figure 4b). This consideration can be supported from the $J-V$ curves in Figure S4 in the Supporting Information, where relatively better photovoltaic characteristics were measured for the device with the P3HT:SiNP-OA active layer compared to the device with the pristine P3HT layer, even though the performance of the P3HT:SiNP-OA device was significantly poorer than the P3HT:$PC_{61}BM$ device. Here it is also noteworthy that the $J-V$ curve shape was the worst for the device with the P3HT:SiNP layer, which can be explained by the poorer dispersion of SiNP than SiNP-OA in the P3HT film.

Finally, we tried to briefly test the stability (lifetime) of the optimized solar cells under continuous illumination of simulated solar light (1 sun, 100 mW/cm^2). As shown in Figure 9, the J_{SC} value of the control device was slowly decreased as the illumination time increased. This decreasing trend is in agreement with our previous work.[28,34,47] Interestingly, the device with 2 wt % SiNP-OA showed almost similar J_{SC} trend with the control device, whereas the J_{SC} value of the device with 2 wt % SiNP was quickly dropped as the illumination time increased. The FF value was also significantly decreased for the device with 2 wt % SiNP, but the device with 2 wt % SiNP-OA showed better FF value than the control device. These results imply that the device performance is critically affected by the dispersion morphology of the active layer which influences on the charge transport characteristics of active layers because of the relatively huge R_S increase for the device with SiNP (see Figure 9 far right panel). In particular, we need to pay our attention to the device with SiNP-OA which exhibited better stability (lifetime) than the control device. As shown in Figure S5 in the Supporting Information, the $J-V$ curve shape of the device with SiNP-OA was kept better than that of the control device, but it became severely

dx.doi.org/10.1021/am301250s | ACS Appl. Mater. Interfaces 2012, 4, 5300−5308

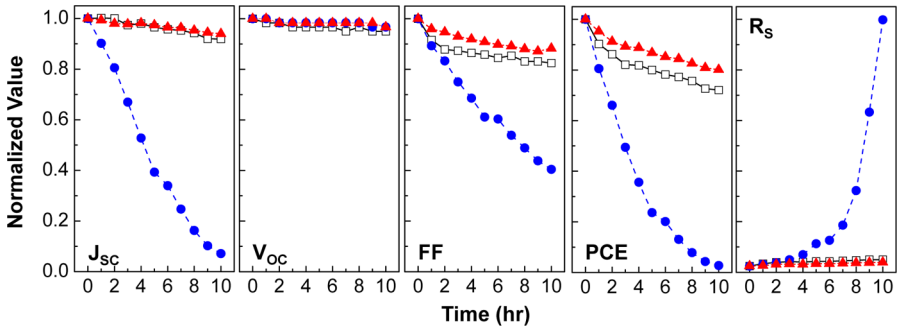

Figure 9. Changes in solar cell parameters of the optimized P3HT:$PC_{61}BM$ solar cells with 2 wt % SiNP or 2 wt % SiNP-OA under continuous illumination of 1 sun: (black open squares) control device (P3HT:$PC_{61}BM$); (blue filled circles) P3HT:$PC_{61}BM$:SiNP_2 wt %; (red filled triangles) P3HT:$PC_{61}BM$:SiNP-OA_2 wt %.

deformed for the device with SiNP. This result strongly supports that the presence of inorganic nanoparticles can improve the stability of organic solar cells if their dispersion morphology could be finely controlled so that the charge transport in the active layer is not disturbed by the presence of inorganic nanoparticles, which can be applied for organic solar cells with thick active layers as well as inverted structrues.[48−50]

■ CONCLUSIONS

The crystalline silicon nanoparticles (SiNP) were chemically modified using octanoic acid (OA) in order to bestow better dispersion in organic solvents. The modification reaction was performed by the mediator-aided esterification between hydroxyl groups (SiNP surfaces) and carboxylic acid groups (OA), which was characterized using Raman spectroscopy and HRTEM. The modified SiNP (SiNP-OA) exhibited considerably better dispersion in chlorobenzene, but the optical absorption, ionization potential and Si crystal nanostructure were almost unchanged upon the esterification reaction. In the case of the unmodified SiNP the device performance was greatly deteriorated upon high loading of SiNP (10 wt %), whereas the modified SiNP (SiNP-OA) delivered relatively good performance without large degradation. The poor device performance in the case of SiNP, compared to the SiNP-OA case, was attributed to the increased series resistance that is assigned to be originated from the coarse morphology as observed from optical microscopy and SEM images even though the long-range order of P3HT crystallites was better for SiNP than SiNP-OA. The optimized devices showed that the device performance was slightly improved by adding 2 wt % SiNP-OA but was degraded by adding 2 wt % SiNP. The short time continuous exposure test under 1 sun condition disclosed that the dispersion morphology did remarkably influence on the stability of solar cells: The device with 2 wt % SiNP-OA showed better stability, whereas the device performance was significantly degraded with the illumination time in the case of 2 wt % SiNP addition.

■ MATERIALS AND METHODS

Chemical Modification of SiNP. The SiNP (size = 20 nm, Nanoarmor Co. Ltd.) was added to the 100 mL flask charged with *N*,*N*-dimethylformamide (DMF), followed by stirring for dispersion. To this solution, 4-(dimethylamino)pyridine (DMAP), *N*,*N*-dicyclohexylcarbodiimide (DCC) and octanoic acid were added and stirred at room temperature for 24 h under nitrogen atmosphere. After stop the reaction, the solution (suspension) was subject to ultracentrifugation and then the precipitates were collected. To remove the unreacted parts (octanoic acid, DMAP, and DCC), the precipitates were poured into methanol and tetrahydrofuran (THF) and dispersed by employing ultrasonication. Then the solid parts were obtained by ultracentrifugation. This purification process was conducted for 4 cycles. Next, to extract the modified SiNP (SiNP-OA), the solid products were dissolved (dispersed) in chlorobenzene (CB) and finally the dissolved parts were collected after 24 h. This solvent part was subject to centrifugation in order to get rid of the rest portion of the unreacted SiNP. Finally, the product dissolved in CB was obtained by removing CB and dried in vacuum at 80 °C.

Preparation of Solutions and Film/Device Fabrication. The regioregular P3HT material (weight average molecular weight ($\bar{M}_w$) = 41 kDa; regioregularity = ∼93%, Rieke Metal Co.) and $PC_{61}BM$ (Nano-C) were used as an electron donor and an electron acceptor, respectively. The binary mixture solution (P3HT:$PC_{61}BM$ = 1:0.7 by weight) for the control device was prepared using CB as a solvent. The ternary mixture solutions (with SiNP or SiNP-OA) were prepared by varying the nanoparticle contents (2, 4, 10 wt %). The solid concentration was fixed as 51 mg/mL. To fabricate solar cells, the indium−tin oxide (ITO)-coated glass substrates (10 Ω/□) were patterned to have 8 mm × 12 mm stripes by employing a photolithography technique, followed by cleaning with acetone and isopropyl alcohol. Prior to the spin-coating process, the cleaned ITO-glass substrates were subject to the UV-ozone treatment. On top of the UV-ozone treated ITO-glass substrates, the hole-collecting buffer layer (thickness = ∼50 nm) was spin-coated using poly(3,4-ethylenedioxythiophene):poly(styrenesulfonate) (PEDOT:PSS) (PH500, Clevios) at 2500 rpm for 1 min and annealed 230 °C for 15 min. Next, the mixture solutions (40 μL) were spun on the PEDOT:PSS layer at 1500 rpm for 30 s, leading to the formation of the active layer (thickness = ∼170 nm). These samples were transferred to a vacuum chamber that is equipped inside an argon-filled glovebox. After pumping down the pressure of the vacuum chamber to 1×10^{-6} Torr, the aluminum (Al) electrodes (thickness =100 nm) were deposited through a shadow mask. All devices were subject to thermal annealing at 140 °C for 30 min and stored inside the glovebox before measurement. For the measurement of Raman spectra, UV−visible absorption spectra, and photoelectron yield spectra, the mixture solutions were spun onto quartz substrates at the same condition as applied for the device fabrication. We note that poly(methyl methacrylate) (PMMA) was employed as a host (matrix) for the measurement of optical absorption spectra.

Measurements. The crystalline nanostructure of SiNP and SiNP-OA was measured using a high resolution transmission electron microscope (HRTEM, Tecnai G2 F20 S-TWIN). The SiNP and SiNP-OA powders were dropped on the copper grid mesh (400 mesh). The Raman spectra of samples were measured using a Raman spectrometer equipped with a Nd:YAG Laser (1000 mW) (Microscopic FT-IR/Raman system, Bruker Optics), while the optical absorption spectra were measured using a UV−visible absorption spectrometer (Optizen 2120UV, Mecasys). The ionization potential of SiNP and SiNP-OA were measured using a photoelectron yield spectrometer (AC2, Hitachi High Tech). The bulk morphology of films was examined using a high-magnification optical microscope

(i.Camscope, Sometech), whereas the surface morphology was measured using a field-emission scanning electron microscope (FESEM S-4800, Hitachi). The nanostructure of the P3HT domains in the films was measured using a synchrotron radiation grazing incidence X-ray diffraction (GIXD) system (9A Beamline, Pohang Accelerator Laboratory, South Korea) (X-ray wavelength = 0.111122 nm, incident angle =0.12°, sample-to-detector distance =238.92 mm). The current density−voltage (J−V) characteristics of solar cells were measured using a specialized solar cell measurement system equipped with an electrometer (Keithley 2400) and a solar simulator (air mass 1.5G filter, 100 mW/cm^2, Newport-Oriel). All measurements were carried out using a nitrogen-filled sample holder that keeps the devices safe from the attack of moisture and/or oxygen. The stability measurement of devices was performed using the same sample holder, which was fixed blow the solar simulator, under 1 sun condition at room temperature.

■ ASSOCIATED CONTENT

Ⓢ Supporting Information

Additional figures (PDF). This material is available free of charge via the Internet at http://pubs.acs.org.

■ AUTHOR INFORMATION

Corresponding Author

**E-mail: ykimm@knu.ac.kr. Tel: +82-53-950-5616.

Notes

The authors declare no competing financial interest.

■ ACKNOWLEDGMENTS

This work was financially supported by Korean Government grants (Basic Research Laboratory Program_2011_0020264, Pioneer Research Center Program_2012-0001262, Priority Research Center Program_2009-0093819, NRF_2012-000523, NRF_2010-0004164). YK acknowledges a special support from Yongjin Fine Chemical Company (Korea) for donating experimental systems.

■ REFERENCES

(1) Tang, C. W. *Appl. Phys. Lett.* **1986**, *48*, 183−185.
(2) Sariciftci, N. S.; Smilowitz, L.; Heeger, A. J.; Wudl, F. *Science* **1992**, *258*, 1474−1476.
(3) Yu, G.; Gao, J.; Hummelen, J. C.; Wudl, F.; Heeger, A. J. *Science* **1995**, *270*, 1789−1791.
(4) Halls, J. J. M; Walsh, C. A; Greenham, N. C.; Marsegla, E. A.; Friend, R. H; Moratti, S. C.; Holmes, A. B. *Nature* **1995**, *376*, 498−500.
(5) Shaheen, S. E.; Brabec, C. J.; Sariciftci, N. S.; Padinger, F.; Fromherz, T. *Appl. Phys. Lett.* **2001**, *78*, 841−843.
(6) Padinger, F.; Rittberger, R. S.; Sariciftci, N. S. *Adv. Funct. Mater.* **2003**, *13*, 85−88.
(7) Brabec, C. J.; Shaheen, S. E.; Wiinder, C.; Sariciftci, N. S.; Denk, P. *Appl. Phys. Lett.* **2002**, *80*, 1288−1290.
(8) Chirvase, D.; Parisi, J.; Hummelen, J. C.; Dyakonov, V. *Nanotechnology* **2004**, *15*, 1317−1323.
(9) Kim, Y.; Cook, S.; Choulis, S. A.; Nelson, J.; Durrant, J. R.; Bradley, D. D. C. Private Communication (2004).
(10) Kim, Y.; Choulis, S. A.; Nelson, J.; Bradley, D. D. C.; Cook, S.; Durrant, J. R. *J. Mater. Sci.* **2005**, *40*, 1371−1376.
(11) Kim, Y.; Choulis., S. A.; Nelson, J.; Bradley, D. D. C.; Cook, S.; Durrant, J. R. *Appl. Phys. Lett.* **2005**, *86*, 063502.
(12) Reyes-Reyes, M.; Kim, K.; Dewald, J.; López-Sandoval, R.; Avadhanual, A.; Curran, S.; Carroll, D. L. *Org. Lett.* **2005**, *7*, 5749−5752.
(13) Li, G.; Shrotriya, V.; Yao, Y.; Yang, Y. *J. Appl. Phys.* **2005**, *98*, 043704−043708.
(14) Ma, W.; Yang, C.; Gong, X.; Lee, K.; Heeger, A. J. *Adv. Funct. Mater.* **2005**, *15*, 1617−1622.
(15) Li, G.; Shrotriya, V.; Huang, J.; Yao, Y.; Moriarty, T.; Emery, K.; Yang, Y. *Nat. Mater.* **2005**, *4*, 864−868.
(16) Kim, Y.; Cook, S.; Tuladhar, S. M.; Choulis, S. A.; Nelson, J.; Durrant, J. R.; Bradley, D. D. C.; Giles, M.; McCulloch, I.; Ha, C.-S.; Ree, M. *Nat. Mater.* **2006**, *5*, 197−203.
(17) Peet, J.; Kim, Y; Coates, N. E.; Ma, W. L.; Moses, D.; Heeger, A. J.; Bazan., G. C. *Nat. Mater.* **2007**, *6*, 497−500.
(18) Chen, H.; Hou, J.; Zhang, S.; Liang, Y.; Yang, G.; Yang, Y.; Yu, L.; Wu, Y.; Li, G. *Nat. Photon.* **2009**, *3*, 649−653.
(19) Dou, L.; You, J.; Yang, J.; Chen, C.; He, Y.; Murase, S.; Moriarty, T.; Emery, K.; Li, G.; Yang, Y. *Nat. Photon.* **2012**, *6*, 180−185.
(20) Hallermann, M.; Como, E. D.; Feldmann, J.; Izquierdo, M.; Filippone, S.; Martin, N.; Jüchter, S.; Hauff, E. V. *Appl. Phys. Lett.* **2010**, *97*, 023301−023303.
(21) Zhao, G.; He, Y.; Li, Y. *Adv. Mater.* **2010**, *22*, 4355−4358.
(22) Jørgensen, M.; Norrman, K.; Krebs, F. C. *Sol. Energy Mater. Sol. Cells* **2008**, *92*, 686−714.
(23) Krebs, F. C.; Spanggaard, H. *Chem. Mater.* **2005**, *17*, 5235−5237.
(24) Neugebauer, H.; Brabec, C.; Hummelen, J. C.; Sariciftci, N. S. *Sol. Energy Mater. Sol. Cells* **2000**, *61*, 35−42.
(25) Kim, Y.; Choi, D.; Lim, H.; Ha, C.-S. *Appl. Phys. Lett.* **2003**, *82*, 2200−2202.
(26) Kim, Y.; Ha, C.-S. *Advances in Organic Light-Emitting Device*; Trans Tech Publications: Zurich, Switzerland, 2008.
(27) Kim, H.; Park, J.; Lee, S.; Ha, C.-S.; Kim, Y. *Sol. Energy Mater. Sol. Cell* **2011**, *95*, 349−351.
(28) Kim, H.; Nam, S.; Lee, H.; Woo, S.; Ha, C.-S.; Ree, M.; Kim, Y. *J. Phys. Chem. C* **2011**, *115*, 13502−13510.
(29) Li, S.-S.; Tu, K.-H.; Lin, C.-C.; Chen, C.-W.; Chhowalla, M. *ACS Nano* **2010**, *4*, 3169−3174.
(30) Irwin, M. D.; Buchholz, D. B.; Hains, A. W.; Chang, R. P. H.; Marks, T. J. *Proc. Natl. Acad. Sci.U.S.A.* **2008**, *105*, 2783−2787.
(31) Scurlock, R. D.; Wang, B.; Ogilby, P. R.; Sheats, J. R.; Clough, R. L. *J. Am. Chem. Soc.* **1995**, *117*, 10194−10202.
(32) Manceau, M.; Rivaton, A.; Gardette, J.-L.; Guillerez, S.; Lemaître, N. *Polym. Deg. Stab.* **2009**, *94*, 898−907.
(33) Shin, M.; Kim, H.; Park, J.; Nam, S.; Heo, K.; Ree, M.; Ha, C.-S.; Kim, Y. *Adv. Funct. Mater.* **2010**, *20*, 748−754.
(34) Kim, H.; Shin, M.; Park, J.; Kim, Y. *ChemSusChem.* **2010**, *3*, 476−480.
(35) Günes, S.; Sariciftci., N. S. *Inorg. Chim. Acta* **2008**, *361*, 581−588.
(36) Kim, Y.; Ha, C.-S.; Chang, T.; Lee, W.-K.; Goh, W.; Kim, H.; Ha, Y.; Ree, M. *J. Nanosci. Nanotechnol.* **2009**, *9*, 4633−4643.
(37) Liu, C.-Y.; Holman, Z. C.; Kortshagen, U. R. *Nano Lett.* **2009**, *9*, 449−452.
(38) Shin, M.; Kim, H.; Nam, S.; Park, J.; Kim, Y. *Energy Environ. Sci.* **2010**, *3*, 1538−1543.
(39) Neises, B.; Steglich, W. *Angew. Chem., Int. Ed.* **1978**, *17*, 522−524.
(40) Zhou, H.; Zhang, C.; Li, H.; Du, Z. *Carbon* **2011**, *49*, 126−132.
(41) Tan, T. T. Y.; Liu, S.; Zhang, Y.; Han, M.-Y.; Selvan, S. T. *Compr. Nanosci. Technol.* **2011**, *5*, 399−441.
(42) Morita, M.; Ohmi, T.; Hasegawa, E.; Kawakami, M.; Ohwada, M. *J. Appl. Phys.* **1990**, *68*, 1272−1281.
(43) Shin, M.; Kim, H.; Kim, Y. *Macromol. Res.* **2010**, *18*, 709−712.
(44) Nam, S.; Lee, S.; Lee, I.; Shin, M.; Kim, H.; Kim, Y. *Nanoscale* **2011**, *3*, 4261−4269.
(45) Kim, H.; Shin, M.; Kim, Y. *Europhys. Lett.* **2008**, *84*, 58002.
(46) Nam, S.; Shin, M.; Kim, H.; Kim, Y. *Nanoscale* **2010**, *2*, 2384−2389.
(47) Lee, S.; Nam, S.; Lee, H.; Kim, H.; Kim, Y. *ChemSusChem.* **2011**, *4*, 1607−1612.
(48) Lee, S.; Nam, S.; Kim, H.; Kim, Y. *Appl. Phys. Lett.* **2010**, *97*, 103503.

(49) Li, G.; Chu, C.-W.; Shrotriya, V.; Huang, J.; Yang, Y. *Appl. Phys. Lett.* **2006**, *88*, 253503−253505.
(50) Chen, L.-M.; Hong, Z.; Li, G.; Yang, Y. *Adv. Mater.* **2009**, *21*, 1434−1449.